Multispectral Photometric Stereo for Acquiring High-Fidelity Surface Normals

Giljoo Nam and Min H. Kim, *Member, IEEE*

***Abstract*—An advanced imaging technique of multispectral imaging has become more accessible as a physically-meaningful image-based measurement tool, and photometric stereo has been commonly practiced for digitizing a 3D shape with simplicity for more than three decades. However, these two imaging techniques have rarely been combined as a 3D imaging application yet. Reconstructing the shape of a 3D object using photometric stereo is still challenging due to the optical phenomena such as indirect illumination, specular reflection, self shadow. In addition, removing interreflection in photometric stereo is a traditional chicken-and-egg problem as we need to account for interreflection without knowing geometry. In this paper, we present a novel multispectral photometric stereo method that allows us to remove interreflection on diffuse materials using multispectral reflectance information. Our proposed method can be easily integrated into an existing photometric stereo system by simply substituting the current camera with a multispectral camera, as our method does not rely on additional structured or colored lights. We demonstrate several benefits of our multispectral photometric stereo method such as removing interreflection and reconstructing the 3D shapes of objects to a high accuracy.**

***Keywords*—multispectral imaging, photometric stereo.**

I. Introduction

Multispectral imaging technology has been practiced for physically-meaningful measurements of radiance as an image, so-called imaging spectroscopy. It has become more accessible nowadays thanks to various imaging technologies such as a liquid crystal tunable filter and a pushbroom camera. In contrast to commodity trichromatic cameras, a multispectral camera yields the multiple channels of spectral power distributions of a surface as a stack of 2D images. Recently, this technique has been more practiced in computer graphics and vision, military, cultural heritage, etc.

Photometric stereo has been commonly performed for capturing the shape of 3D solid objects in computer vision for more than three decades. While binocular stereo estimates the depth information using two cameras with static illumination, photometric stereo estimates the surface normal information of the object using a single camera with varying lighting conditions. Photometric stereo can provide a high-resolution normal map with simplicity and convenience. However, multispectral imaging and photometric stereo have been rarely practiced together in the multispectral imaging and computer vision domains. In photometric stereo, many optical phenomena occur as obstacles, such as indirect illumination, specular reflection and self shadows, degrading the accuracy of the shape measured by photometric stereo. Since photometric stereo was introduced [1], many researchers worked on reconstructing surface normals from non-Lambertian reflections by removing self shadow and specular reflection in photometric stereo [2]. However, removing the indirect illumination effect in photometric stereo [3], [4] has been less discussed. Interreflection occurs when two points over a concave surface face to each other. Most photometric stereo algorithms are designed in the general assumption of Lambertian reflection on convex shapes, which do not suffer from interreflection. However, objects in the real world are built with a mixture of convex and concave shapes.

Removing interreflection is challenging as the effect is integrated in a light path. The second-bounded light is affected by the surface albedo of the reflecting surface. The second-bounded light becomes a new light source and the reflection is added on each point. Most of energy that comes into the camera is either direct from the light source or one bounded light from the object surface, which is the inner product of the light and surface reflectance. The portion of second and higher bounded light varies from the scene. Some object or scene are more vulnerable to the indirect illumination. In this case, the radiance measured by a camera is affected not only by the illumination and the surface albedo, but also by the reflectance of the surrounding surfaces.

In this paper, we present a novel method for removing interreflection in *multispectral photometric stereo*. We model multiple bounces of *wavelength-dependent* interreflection as a polynomial function and optimize the interreflection effect through multispectral reflectance analysis. This allows us to separate interreflection over diffuse surfaces from measured radiance. Our multispectral photometric stereo does not rely on multiplexing spectral lights like [5], [6], i.e., our proposed method works on arbitrary shape and illumination without help of structured light and colored light. To our best knowledge, this is the first such attempt for removing interreflection in multispectral photometric stereo. We demonstrate the usefulness of our multispectral photometric stereo to measure the shape of monochromatic 3D solid objects such as a human face to a high accuracy. Our interreflection removal method can be easily integrated into existing photometric stereo systems even with a commodity trichromatic camera (though becomes less powerful) while not modifying light sources. Figure 1 presents an overview of our multispectral photometric stereo method.

II. Related Work

This section briefly overviews relevant previous work in multispectral imaging and photometric stereo.

G. Nam and M.H. Kim (corresponding author) are with the Department of Computer Science, KAIST (Korea Advanced Institute of Science and Technology), Daejeon, 305-701, South Korea, e-mail: minhkim@kaist.ac.kr

Manuscript received April 7, 2014; revised August 13, 2014.

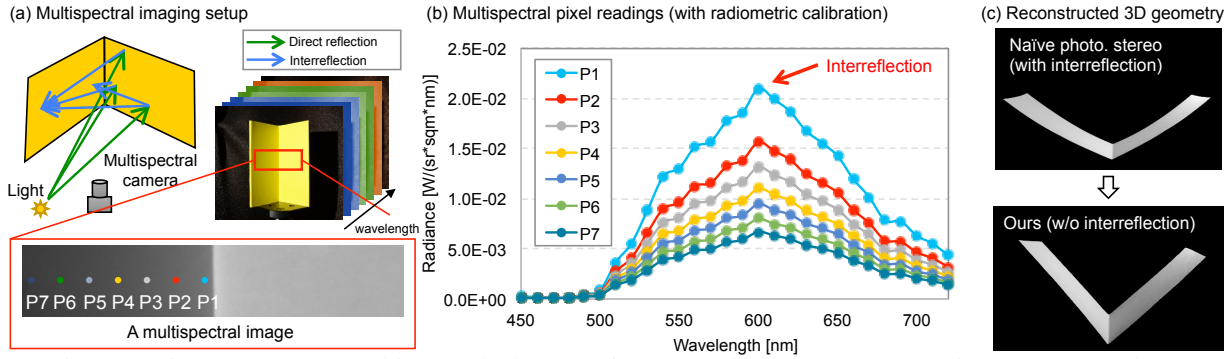

Fig. 1: *Schematic diagram of our* multispectral photometric stereo *that removes interreflection effectively. (a) shows the measurement setup and captured image of the target object (L-shaped in 90°). The inner faces of the object present interreflection along with direct reflection. (b) presents the radiometric power distribution (captured by a multispectral camera) over the seven points on the left-hand-side surface with interreflection. (c) compares the reconstructed 3D geometries using ordinary photometric stereo with interreflection and our method that removes interreflection using multispectral photometric stereo.*

A. Multispectral Imaging

Multispectral imaging is often called as imaging spectroscopy, where a pixel in a spectral image indicates spectral power per wavelength to present spatial variation of spectrum on captured radiant flux. A bandpass filter [7] or dispersion unit [8] is commonly employed to build a multispectral imaging system.

BANDPASS-BASED IMAGING. A bandpass filter-based imaging system includes a set of narrow bandpass filters on a wheel or liquid crystal tunable filter (LCTF) [7] in its optical path. A monochromatic sensor captures the energy of a certain frequency band through a bandpass filter, where the spectral resolving power depends on the bandwidth of the filter. The minimum bandwidth of a general optical filter is about 10 – 15 nm. Recently, Takatani et al. [5] introduced a photometric stereo method using multispectral imaging. They enhanced the surface normals by segmenting multispectral image data and identifying a wavelength per segment patch that fits the most to the Lambertian constraints. However, they did not concern the interreflection effect while reconstructing the normals.

DISPERSION-BASED IMAGING. A dispersion-based spectral imaging system includes a slit and a dispersion unit like a prism [8]. The imaging system measures the dispersed spectrum and reconstructs three-dimensional spectral data. Pushbroom cameras, where either a slit or a sensor needs to be moved mechanically to obtain spectral images, are commonly used. A drawback of this type is that the spatial resolution of the spectral images in the mechanically moving direction is lower than the other direction. Snapshot-based systems have been proposed as an alternative that allows to capture moving objects. Recently such a multispectral imaging systems have been combined with a 3D laser scanning technology [9] to open a new paradigm of spectral measurements.

MULTIPLEXING SPECTRAL IMAGING. Multiplexing of narrow-band spectra is an alternative for multispectral imaging. A series of narrow-band LED lights in general is coupled with a monochromatic camera. This configuration enables to capture multispectral reflection from the multispectral light source. Recently Vogiatzis and Hernandez [6] introduced a multiplexing-light based photometric stereo method that allows to capture 3D animation using a structure-from-motion approach.

B. Removing Interreflection in Photometric Stereo

Photometric stereo, known as *shape-from-shading*, estimates surface gradients using images taken under multiple light directions, assuming that the surface reflection observes the Lambertian constraints. As interreflection breaks this assumption, which is critical for photometric stereo, there has been a few work on removing interreflection in photometric stereo.

ACTIVE APPROACH USING STRUCTURED LIGHT. Nayar et al. [10] introduced a seminal work to remove interreflection using structured light patterns. They used a high frequency illumination pattern in order to separate the direct and indirect illuminations of a scene. While two illumination patterns are enough to separate the indirect illumination theoretically, three illumination patterns were used in practice. For photometric stereo, they used the high frequency illumination patterns for each light sources; thus at least triple-number of images were required.

INTERREFLECTION MODELS. Nayar et al. [3] presented an iterative method to estimate non-biased surface normals. They first estimated a pseudo shape, a shape that contains interreflection in its shape and reflectance, and iteratively corrected the pseudo shape so that it converges to the real shape. They also showed the convergence property of their iterative algorithm. Liao et al. [4] presented an active method to remove n-bounded light in photometric stereo using colored multiplex lighting. The proposed algorithm theoretically assumes that there are at least two images of an object with same illumination but varying surface albedos. However, this assumption is technically impossible in the real world. Instead, they changed illumination spectrum to emulate the changes of surface albedo. They modeled and solved an interreflection model based on monochromatic surface albedo.

Most of prior interreflection-removal methods have employed active approaches with the specially designed illumination patterns or the spectrum of the modified light sources. In contrast,

PRELIMINARIES

INTERREFLECTION

When a beam of light strikes a diffuse surface of a color, iterative scattering occurs between neighboring surfaces. We call this phenomenon *interreflection*. Interreflection always occurs along the surface of media when a concave shape is illuminated.

Kajiya [1] models recursive light transport w.r.t. the incident Ψ and exitant Θ light directions in the hemispherical domain as a rendering equation:

$$L(x \to \Theta) = L_e(x \to \Theta) + \int_{\Omega_x} \rho(x, \Psi \to \Theta) L(x \leftarrow \Psi) cos(N_x, \Psi) d\omega_\Psi \,,$$

where $\rho()$ is a reflectance function; N_x is a surface normal at the point x.

In a diffuse environment, self-emitted radiance $L_e()$ and reflectance $\rho()$ do not depend on the incident and exitant light directions. Although the incident radiance, say $L(x \leftarrow \Theta')$, still depends on incident direction, the light transport on purely diffuse surfaces can be simplified:

$$L(x) = L_e(x) + \int_{\Omega_x} \rho(x) L(x \leftarrow \Theta') \cos(N_x, \Theta') d\omega_{\Theta'}.$$

The spherical integral over the hemisphere Ω_x can be transformed into an integral over all surfaces S in the scene. Hence no directions appear anymore in the rendering equation:

$$L(x) = L_e(x) + \rho(x) \int_S K(x,y) L(y) dA_y,$$

where $K(x,y)$ is the product of a binary visibility $V(x,y)$ and the geometrical relationship $G(x,y)$ between the illuminating surface y and the reflected surface x at a distance r: $G(x,y) = \cos(N_x, \Theta') \cos(N_y, -\Theta') / {r_{xy}}^2$.

We now rewrite the above in a discrete matrix-vector form:

$$L = L_e + (\rho K) L, \tag{1}$$

where L is a radiance vector of each infinitesimal patch dA, L_e is a self-emitted radiance vector of each patch, and ρK is an exitant diffuse illumination vector (so-called radiosity). Assuming a state of equilibrium for light transfer, we can rewrite Eq. (1) as $L = (I - \rho K)^{-1} L_e$. Again we can expand this into a Neumann series:

$$L = L_e + (\rho K) L_e + (\rho K)^2 L_e + \cdots + (\rho K)^n L_e. \tag{2}$$

In this form, we can easily model how much light energy is contributed from n-bounded light; n-th order of the polynomial is equivalent to the effect of n-bounded light. This allows us to remove indirection illumination from reflection.

PHOTOMETRIC STEREO

A shading illuminated by a point light I can be calculated as a dot product between the incident radiance L and surface normal N: $I = L \cdot N$.

Suppose we obtain i images under a different light in photometric illumination, we can obtain the following linear system for each point of the surface:

$$\begin{bmatrix} I_1 \\ I_2 \\ \vdots \\ I_i \end{bmatrix} = \begin{bmatrix} L_{1,x} & L_{1,y} & L_{1,z} \\ L_{2,x} & L_{2,y} & L_{2,z} \\ & \vdots & \\ L_{i,x} & L_{i,y} & L_{i,z} \end{bmatrix} \begin{bmatrix} N_x \\ N_y \\ N_z \end{bmatrix}.$$

To solve the linear system above, the row-rank of the matrix L should be at least three. With more than three light sources used, it becomes an over-constrained linear system and can be solved using least-squares to obtain a normal estimate N.

SHAPE FROM NORMALS

Once we obtain a surface normal per pixel, each point on the image now has a normal N of $\{N_x, N_y, N_z\}$; therefore, we solve for the height field z at (x,y) by minimizing an objective function [2]:

$$\Gamma(z) = \sum_{x,y} \left(N_z \frac{\partial z(x,y)}{\partial x} + N_x \right)^2 + \left(N_z \frac{\partial z(x,y)}{\partial y} + N_y \right)^2.$$

where we approximate the ratios of the partial derivatives of z to x and y assuming orthographic projection:

$$\frac{\partial z(x,y)}{\partial x} = z(x+1, y) - z(x,y);$$
$$\frac{\partial z(x,y)}{\partial y} = z(x, y+1) - z(x,y).$$

Once we obtain a set of point clouds (a set of $\{x, y, z\}$), we recover a 3D shape of the surface by indexing neighboring points.

REFERENCES

[1] J. T. Kajiya, "The rendering equation," in *Proc. ACM SIGGRAPH Computer Graphics '86*, vol. 20, no. 4, 1986, pp. 143–150.

[2] R. Basri, D. W. Jacobs, and I. Kemelmacher, "Photometric stereo with general, unknown lighting," *Int. J. Comput. Vision (IJCV)*, vol. 72, no. 3, 2007.

we propose a channel separation technique in multispectral imaging without relying on active lighting approach. Therefore, our passive method can be easily integrated into any previous photometric stereo systems and remote sensing systems. To our best knowledge, this is the first such attempt for removing interreflection in multispectral photometric stereo.

III. MULTISPECTRAL PHOTOMETRIC STEREO

Our objective is to remove interreflection prior to reconstructing surface normals using photometric stereo.

A. Multispectral Interreflection Removal

The interreflection of n-bounded light increases reflected energy consistently as an n-th order polynomial function [4]. We extend this idea to the *wavelength-dependent reflectance* of the n-th order bounce, which is captured by a multispectral imager. By excluding the self-emitted radiance (the first term) from the global illumination in Eq. (2), we can define pure reflected radiance L' as a polynomial function of reflectance (ρK):

$$L' = (\rho K) L_e + (\rho K)^2 L_e + \cdots + (\rho K)^n L_e. \tag{3}$$

Now distinguishing direct and indirect illumination is equivalent to identifying each term of this polynomials.

Liao et al. [4] conducted a seminal experiment and proved this mathematical derivation by illuminating a monochromatic surface with *an RGB projector*. However, it is prohibitively demanding to take the images of the same object with different reflectance values while maintaining the geometry. In contrast,

we explore this idea in aspects of multispectral imaging. We mainly benefit from the fact that most materials in the real world have different reflectances in different wavelengths, except for a Spectralon tile. We treat each wavelength channel as an independent observation with different illumination and reflectance respectively. This allows us to distinguish n-bounded light using multiple observation of individual multispectral channels of the same surface without relying on multiplexing of light or albedo [4]. Now we can extend Eq. (3) as a series of n-th order polynomials with multispectral channels λ:

$$\begin{aligned} L'_1 &= \rho_1 L_{e,1} K + {\rho_1}^2 L_{e,1} K^2 + \cdots + {\rho_1}^n L_{e,1} K^n \\ L'_2 &= \rho_2 L_{e,2} K + {\rho_2}^2 L_{e,2} K^2 + \cdots + {\rho_2}^n L_{e,2} K^n \\ &\vdots \\ L'_\lambda &= \rho_\lambda L_{e,\lambda} K + {\rho_\lambda}^2 L_{e,2} K^2 + \cdots + {\rho_\lambda}^n L_{e,n} K^n . \end{aligned}$$

We can rewrite this as a linear system equation:

$$\begin{bmatrix} L'_1 \\ L'_2 \\ \vdots \\ L'_\lambda \end{bmatrix} = \begin{bmatrix} L_{e,1}\rho_1 & L_{e,1}{\rho_1}^2 & \cdots & L_{e,1}{\rho_1}^n \\ L_{e,2}\rho_2 & L_{e,2}{\rho_2}^2 & \cdots & L_{e,2}{\rho_2}^n \\ \vdots & \vdots & \ddots & \vdots \\ L_{e,\lambda}\rho_\lambda & L_{e,\lambda}{\rho_\lambda}^2 & \cdots & L_{e,\lambda}{\rho_\lambda}^n \end{bmatrix} \begin{bmatrix} K \\ K^2 \\ \vdots \\ K^n \end{bmatrix} .$$

It is worth noting that the spectral profile of illumination L_e is multiplied with the reflectance polynomials ρ. We can obtain these two properties from the set of multispectral images by taking pictures of the object with a Spectralon reference tile together. Now let's simplify it in a matrix-vector form:

$$L' = RA, \tag{4}$$

where L' is a multispectral radiance vector of interreflection; R is an element-wise multiplication of the illumination and the reflectance polynomials; A is a vector of polynomials of form factors. To solve Eq. (4), we calculate A by minimizing the following objective function $O(A)$:

$$O(A) = ||L' - RA||_2^2 . \tag{5}$$

In our system, the row-rank of λ (e.g., 29 channels) is higher than n (the order of bounces). It becomes an over-constrained linear system, which can be solved by a general least-squares optimization method such as QR decomposition or SVD. Although our method in theory can solve the same order of bounces as the number of the multispectral channels, we cut off the terms higher than a certain number of bounces because they are physically and numerically negligible in our experiment.

B. A Multispectral Photometric Stereo System

Our imaging system comprises two main folds: a multispectral imager and a computer-controlled photometric lighting system.

MULTISPECTRAL IMAGER. We built a multispectral imager, which consists of an LCTF (Varispec VIS0720), a monochromatic camera (Point Grey FL3-GE-13S2M-C) and a Nikon F-mount lens. The monochromatic camera includes a 14-bit analog-to-digital converter (ADC). Hence, we output 16-bit RAW images so that we can make use of full performance of the sensor. We turned off gamma-correction as it yields non-linear camera response to the incident radiance. A linear camera response is a matter of great importance in the following camera calibration process. We carefully chose the focal length of the lens to avoid the vignetting effect caused by the LCTF in front of the objective lens. Note that we treat each channel as if it is an independent scene with its own irradiance and reflectance but theoretically on a same geometry, e.g., in Figure 3, we regard the 550 nm channel shows a part of the scene that has the same irradiance level with the 650 nm channel and one-tenth of reflectance than the 650 nm channel of the same geometry.

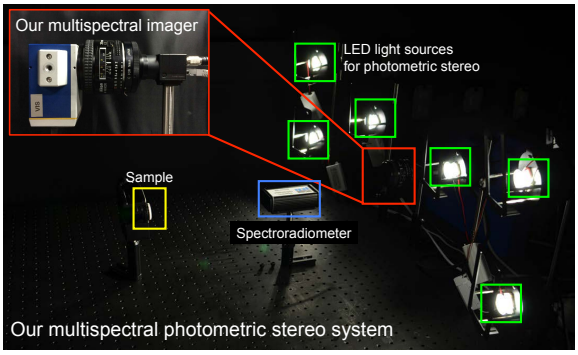

Fig. 2: *Our multispectral photometric stereo system. We configure this imaging system with our custom-built multispectral imager and six visible LED light sources.*

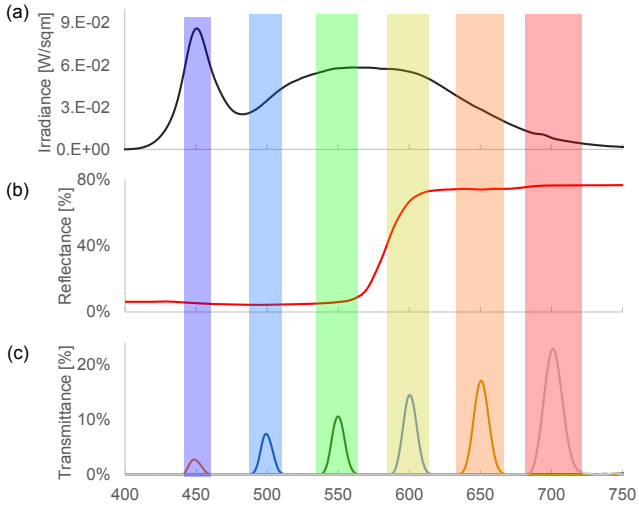

(d)

Wavelength [nm]	450	500	550	600	650	700
Irradiance [W/sqm]	0.72	0.31	0.60	0.60	0.60	0.16
Reflectance [%]	5	4	6	50	74	77
Bandwidth [nm]	9	12	16	20	23	31

Fig. 3: *An example of radiometric measurements by our multispectral imager. (a) presents the measured irradiance of the LED lights for photometric stereo. (b) shows the reflectance of a red patch. (c) describes the measured transmittance in 50 nm intervals of the LCTF filter. (d) compares the irradiance, reflectance and the bandwidth of each channel.*

PHOTOMETRIC LIGHTING SYSTEM. We complete a multispectral photometric stereo system, which consists of six LEDs as light sources and the multispectral imager. We chose CREE CXA1512 high power LED coupled with a heat sink. The LED with heat sink provides a stable illumination, less time varying,

and no peak spectrum. The lights are positioned at a distance of 0.62 m—1.00 m from the target object. Our system setup is illustrated in Figure 2.

C. System Calibration

RADIOMETRIC CALIBRATION. We calibrate our multispectral imager radiometrically in order to measure physically-meaningful radiance. Given upon the linear responses of the image sensor, we determine a linear transformation per wavelength between incident radiance and camera signals as an inverse camera response function, yielding radiance.

For radiometric calibration, we use an X-rite ColorChecker with 24 color patches with known reflectances. Two LED lamps illuminate the ColorChecker at 45 degrees of both sides. A spectroradiometer (Jeti Specbos 1200) and our multispectral camera measure the reflected radiance and the camera sensor signal respectively. We find a linear mapping function using two measurements while taking account of the measured transmittance of LCTF [11]. Once we calibrate the multispectral camera, we can measure the physically-meaningful radiance of an arbitrary scene with the camera sensor signal by scaling, i.e., our multispectral imager captures physically-meaningful radiance images like a 2D spectroradiometer.

GEOMETRIC CALIBRATION. Geometric calibration for the positions of point lights is necessary for photometric stereo. The specular reflection of a point on a chrome ball (with a known diameter) indicates a reflected light R about the normal vector N. Using the symmetry of the law of reflection, we can determine the light direction L with respect to the viewing direction (same as R), solving a linear equation: $R = 2(N \cdot L)N - L$. We calibrate the light vectors for all the point lights.

D. Experimental Procedure

The experimental procedure is as follows. First, we capture multispectral images of an object with our multispectral camera for each light source and save the multispectral images in OpenEXR format files. The multispectral reflectance of the monochromatic surface can be obtained by capturing a Spectralon (99% calibrated) alongside the object. The intensity ratio between the convex area of the object and the Spectralon becomes the precise multispectral reflectance of the object at a certain wavelength. Note that in this way, the reflectance of the object need not to be a known property before the acquisition but can be obtained during the acquisition. Second, we perform multispectral interreflection removal for each multispectral image. Third, we perform photometric stereo using interreflection-free images and obtain a surface normal map of the object. As we use an LED light as a point light source at a distance of less than a meter, the light does not illuminate the object surface uniformly. In order to compensate this effect, we capture a white diffuse plate and create an illumination profile to cancel out the spatial variation of the irradiance. Finally, we reconstruct the 3D shape of the object using the normal map.

IV. RESULTS

In order to recover a 3D shape, our multispectral photometric stereo system captures six multispectral images of 29 channels, from 440 nm to 720 nm in 10 nm intervals, with the LED lights at different positions (see Figure 2). We then perform the proposed multispectral interreflection removal method and apply photometric stereo with the images exclusively under direct illumination.

A. Separating Direct and Indirect Illumination

We first evaluate our multispectral interreflection algorithm with ground truth data generated by a multispectral path-tracing renderer, Mitsuba [12]. We simulated multispectral light transports with the same configuration of our multispectral photometric stereo imaging acquisition.

Figure 4 presents the results of our simulation: Happy Buddha with a sphere. We created a synthetic scene with a monochromatic color of an orange color, lit under directional lights, of which the spectral power distribution is same as that of an LED light used in our physical experiments. In addition to the target scene, we added a reference white object to calculate the reflectance of the scene objects. We performed our interreflection removal method up to fourth-bounces and then separated them from the direct reflection. As shown in (a), the concave areas of the object and the corner between the two walls are brighter than the neighboring areas due to the interreflection. (b) and (c) present the results of our multispectral interreflection removal. We compare the peak signal-to-noise ratio (PSNR) between our direct illumination estimate (b) and the rendering of direct illumination only (d). When computing the PSNR, we use an image of the 600 nm wavelength as it records the highest signal and is used as an input in photometric stereo after the interreflection effect being removed. Our method yields virtually identical estimates of the direct illumination to the reference when we compute more than third-bounded illumination.

We also compared our simulation result with that of Liao et al. [4]. The same scene was lit by different colored lights, i.e., red, green, blue, cyan, magenta, and yellow, to determine the wavelength-dependent reflectance of the objects. The remaining part of the interreflection removal algorithm is the same as ours. (e) demonstrates that our method outperforms the active method [4] regardless of the number of bounces.

B. Accuracy in Acquiring a 3D Shape

An L-shaped object has been used in evaluating interreflection removal algorithms as its geometry is known as 90° of internal angle between two faces [3], [4]. We also evaluate the geometric accuracy of our system, using a physically L-shaped object with a diffuse color.

Figure 5 compares the reconstructed internal angle between the two faces of an L-shaped object. (a) and (b) show the 3D geometries of the object with and without interreflection. (a) shows a less concave shape while (b) shows a flat surface, a sharp edge, and an accurate internal angle. The internal angle was calculated by averaging the angles between two normal vectors

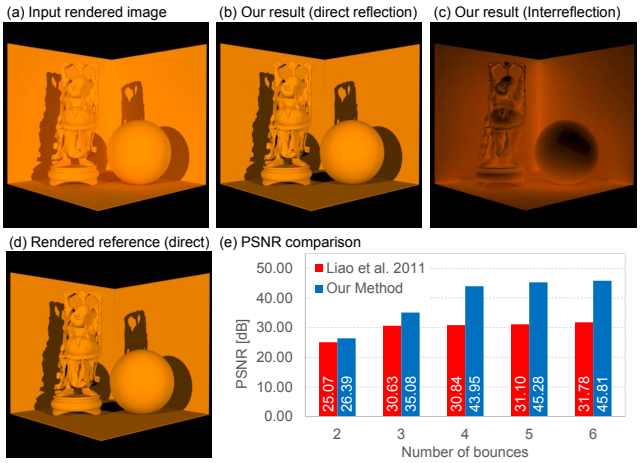

Fig. 4: *Direct/indirect illumination separation with multispectral rendering. A scene with an orange color is rendered under the spectrum of our LED light using a multispectral path tracer [12]. (a) the input rendered image. The sRGB values are computed from the spectral power distribution for visualization. (b) our direct reflection image (up to fourth bounces). (c) interreflection effect separated by our method. (d) the rendered reference of direct reflection. (e) PSNR comparison with Liao et al. [4]. The PSNR of the 600 nm wavelength is computed between the rendered reference of direct reflection and the estimation of each method. Our method outperforms the active method [4].*

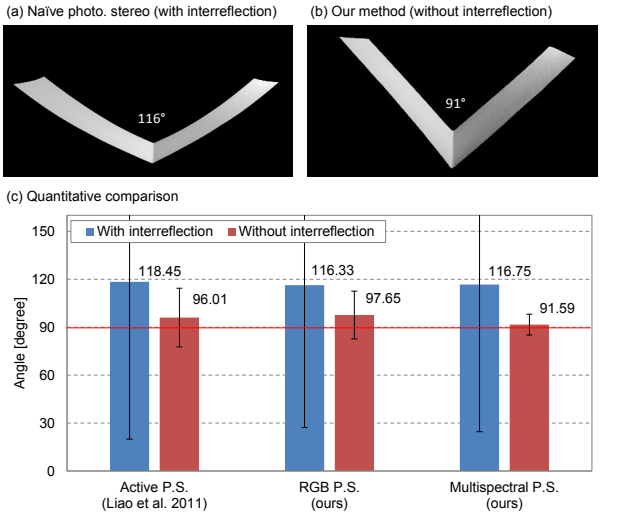

Fig. 5: *Comparison of the reconstructed geometry (a physical angle measure: 90°). (a) a reconstructed geometry using a naïve photometric stereo method with interreflection. (b) a 3D shape reconstructed by our multispectral photometric stereo. (c) quantitatively compares the estimated internal angle among an projector-based active photometric stereo method [4], our method (using an RGB camera), and our multispectral method.*

on each symmetric side of the L-shaped object on the normal map. When interreflection was removed, the internal angle was improved by 16.75% on average for the four test colors: yellow, red, green, and blue. In addition, we compare the performance of our interreflection removal method with an ordinary RGB camera. We calibrate the RGB camera radiometrically and apply our proposed method for this trichromatic input. (c) compares the performance of our multispectral method with our method with an RGB camera and an active photometric stereo method with a beam projector [4]. Our method using the multispectral imager yields a highly accurate internal angle (91.59°) with smaller deviation (σ=6.51°) than the active method [4] (96.01°, σ=18.35°). As we calculate the internal angle pixel-by-pixel, larger deviation implies larger noise, i.e., our multispectral method performs better than the others. We could trace back this result caused by the wide spectral bandwidth of the trichromatic camera (roughly 100 nm—200 nm per channel). Using wide sensing bandwidth suffers from loosing the spectral details of wavelength-dependent reflectance as metamerism.

C. Scanning 3D Objects

This section demonstrates 3D scanning applications with several 3D objects. Figure 6 compares the performance variation of our method according to the number of input spectral channels. We scan a concave-shaped soap, which can maximize the interreflection. As a soap has specular reflection, polarizing filters are attached in front of light sources in order to prevent the specular reflection comes into the sensor directly. We compare three different 3D photometric stereo results to the ground truth obtained by a 3D laser scanner (NextEngine). (b) shows the reconstruction results of the normals and 3D geometry with the naïve photometric stereo approach (without removing interreflection). The reconstructed geometry is flatten compared to the ground truth. (c) and (d) present the normals and 3D models using our method with two different cameras: an RGB camera and our multispectral imager. In (c), although the reconstructed geometry is still somewhat flattened, there is an improvement in terms of sharpness on the edges. (d) shows the results of our multispectral photometric stereo system using 29 channels. Our multispectral method yields a virtually identical geometry to the ground truth. Using a sufficient number of channels, our method can acquire high-frequency details of the object surface, yielding high-fidelity normals and 3D shapes.

We estimate a normal map and reconstruct the geometry of a plaster figure of David. A plaster figure in a white color has virtually uniform reflectance per wavelength, which would reduce the stability of the linear system in Eq. (4). Thus, we coat the plaster with a diffuse red paint to intensify the reflectance difference among the spectral channels. Figure 7 compares the normal map and the 3D geometry model reconstructed by (a) a 3D scanner, NextEngine, (b) Liao et al. [4] and (c) our multispectral photometric stereo. The curly hair of the figure makes it difficult to estimate accurate surface normals due to the interreflection. As the 3D scanner utilizes the triangulation method to reconstruct the geometry, its output is considered as a ground truth geometry even though it struggles with occlusion around the concave faces. Our multispectral photometric stereo system yields accurate surface normals and provides geometrical details as much as the ground truth.

Figure 8 shows the results of scanning a human face. Facial

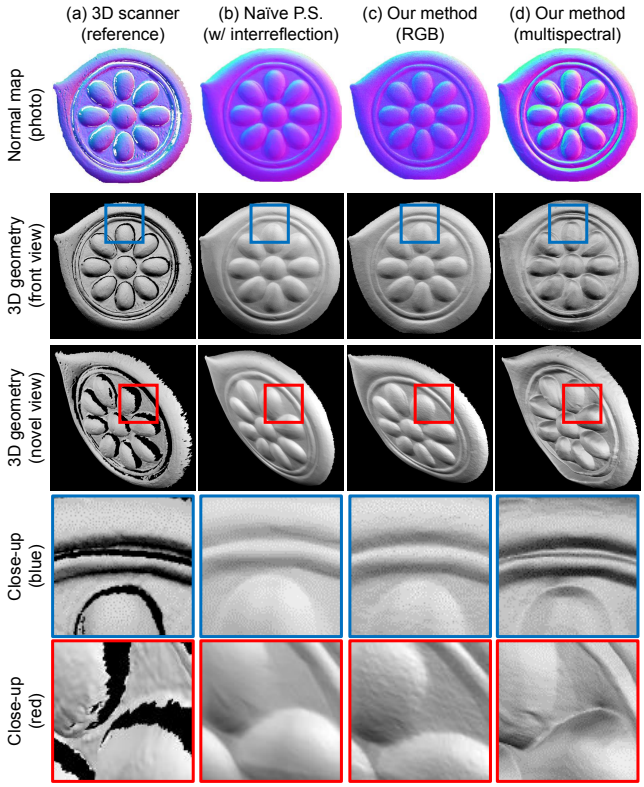

Fig. 6: *Comparison of the reconstructed 3D models depending on the number of input spectral channels. (a) The ground truth obtained by a 3D laser scanner (NextEngine). (b) A naïve photometric stereo without removing interreflection. (c) Applying our multispectral method to an RGB camera using three spectral channels. (d) Our multispectral photometric stereo using 29 channels. The reconstructed shape is virtually identical to the ground truth.*

features, such as a nose, a mouth and eyes, make the overall shape of the face a mixture of concave and convex areas. In particular, the area between two eyes, the area between a nose and a cheek and the area between two lips are vulnerable to the interreflection. In addition, the rough skin also produces the interreflection in a micro scale. (a) and (b) compare the results of the naïve photometric stereo and those of our multispectral photometric stereo. The reconstructed geometry in (a) shows a flattened facial shape and a smooth skin. In contrast, in (b), the concavity, as well as the convexity, of the face are well preserved and the skin keeps the roughness of the human skin. (c) and (d) show the close-ups of (a) and (b), respectively. Note that, tiny features in the skin, such as acne, are blurred in (c) and only recovered by our method in (d).

V. Discussion

Our multispectral photometric stereo system captures surface normals to a high accuracy by removing interreflection over monochromatic diffuse surface. This allows us to reconstruct 3D geometry models with a high accuracy. A virtue of our system is that it is not tied to a specially designed illumination, e.g., structured light patterns or spectral light controls, and thus

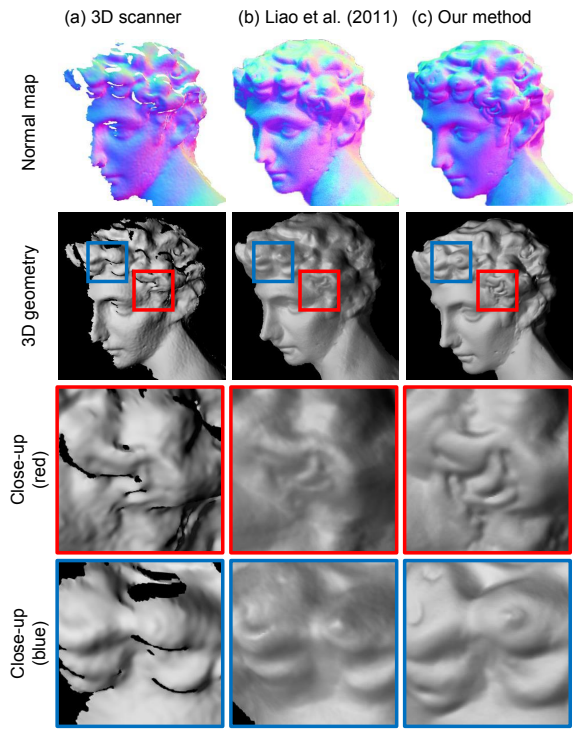

Fig. 7: *Comparison among the results of (a) a 3D scanner (reference), (b) projector-based photometric stereo (Liao et al. [4]) and (c) our multispectral photometric stereo. Our method yields better surface normals and the 3D model compared to the active method. The 3D model reconstructed by our method includes details as much as the reference even without occlusion.*

can be applied in any existing photometric stereo system by adding a multispectral camera. We expect our method provides an easy solution, i.e., adding a multispectral camera, to upgrade existing photometric stereo systems such as facial scanning systems or industrial vision inspection systems.

However, some limitations still remain. Our geometric calibration of illumination does not account for the parallax effect of the light source. We used an LED light as a point light source in less than a meter for power efficiency; hence, the directions of all the rays from a light source are not perfectly parallel along the light transport path.

Our method functions on the assumptions that the surface albedo of the target object must be monochromatic and that the surface albedo must also have different ratios per wavelength. In practice, a color opaque spray has been frequently practiced for high-precision 3D scanning, where our method can obtain the high-fidelity surface normals at the cost of using a spray.

The acquisition time is proportional to the number of channels we capture. In future work, we will use a dispersion-based multispectral imager like [9]. Using a dispersion-based multispectral imager with enough spatial resolution, it is possible to capture a video sequence of moving objects without suffering from interreflection.

Finally, although the performance of our interreflection removal algorithm increases with the number of bounces in the

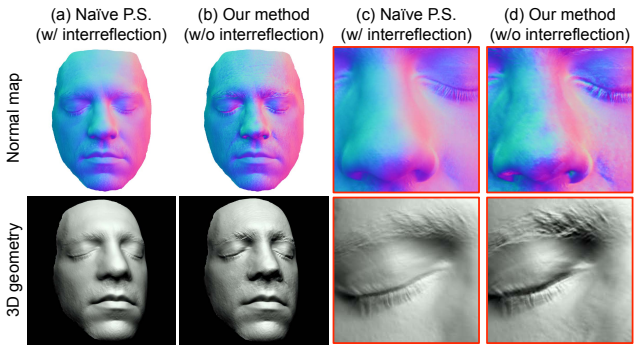

Fig. 8: *Results of scanning a human face. (a) shows the normal map and the reconstructed 3D geometry using naïve photometric stereo. (b) shows the results from our multispectral photometric stereo. (b) presents the concavity and the convexity of the facial features better than (a). In addition, the roughness of the human skin is well recovered in (b). (c) and (d) show the close-ups of (a) and (b), respectively. Note that, tiny features in the skin, e.g., acne, are only recovered by our method in (d).*

multispectral rendering simulation (see Figure 5), we found that the second-bounded model produces the most accurate results in the physical experiment with a camera. When we took account of more than third-bounded light, we encountered an overfitting problem with some scenes at times. We infer that this is due to several practical imaging issues including the sensor noise, the highly sensitive spectral transmittance of the LCTF, specular reflections on a surface, strong self-shadowing areas, low emission values of a light source for specific wavelength, etc. Taking only the first two terms in Eq. (3) could compensate the aforementioned problems and improve the numerical stability of our method. One way to further overcome these issues as future work is to use a conditional iterative optimization method.

VI. Conclusion

We present a novel multispectral photometric stereo method that allows us to remove indirect illumination from reflection and to reconstruct high-fidelity surface normals and geometry exclusively from direct illumination to a high accuracy. We validate the performance of our method, compared with other projector-based approaches in terms of 3D geometry. In contrast to other projector-based approaches, our method could be easily integrated to the existing photometric stereo systems by simply substituting the RGB camera with a multispectral camera. We have demonstrated its usefulness for high-fidelity geometric acquisition in forms of surface normals and 3D models.

Acknowledgment

Min H. Kim gratefully acknowledges support from the National Research Foundation of Korea (2013R1A1A1010165 and 2013M3A6A6073718) and additional support from Microsoft Research Asia. The authors appreciate valuable comments on this work by Xin Tong and Steven Lin (MSRA), and Michael Dobbins (KAIST) for participating the 3D scanning experiment.

References

[1] R. Basri, D. W. Jacobs, and I. Kemelmacher, "Photometric stereo with general, unknown lighting," *Int. J. Comput. Vision*, vol. 72, no. 3, 2007.

[2] F. Verbiest and L. Van Gool, "Photometric stereo with coherent outlier handling and confidence estimation," in *Proc. Comput. Vision and Pattern Recognition (CVPR)*, 2008, pp. 1–8.

[3] S. K. Nayar, K. Ikeuchi, and T. Kanade, "Shape from interreflections," *Int. J. Comput. Vision (IJCV)*, vol. 6, no. 3, pp. 173–195, 1991.

[4] M. Liao, X. Huang, and R. Yang, "Interreflection removal for photometric stereo by using spectrum-dependent albedo," in *Proc. Comput. Vision & Pattern Recognition (CVPR)*, 2011, pp. 689–696.

[5] T. Takatani, Y. Matsushita, S. Lin, Y. Mukaigawa, and Y. Yagi, "Enhanced photometric stereo with multispectral images," in *Int. Conf. Machine Vision Applications (MVA)*. IAPR, 2013.

[6] G. Vogiatzis and C. Hernández, "Self-calibrated, multi-spectral photometric stereo for 3d face capture," *Int. J. Comput. Vision (IJCV)*, vol. 97, no. 1, pp. 91–103, 2012.

[7] H. Lee and M. H. Kim, "Building a two-way hyperspectral imaging system with liquid crystal tunable filters," in *Springer LNCS 8509 (Proc. ICISP 2014)*. Normandy, France: Springer, 2014, pp. 26–34.

[8] P. Mouroulis, R. O. Green, and T. G. Chrien, "Design of pushbroom imaging spectrometers for optimum recovery of spectroscopic and spatial information," *Applied Optics*, vol. 39, no. 13, pp. 2210–2220, 2000.

[9] M. H. Kim, T. A. Harvey, D. S. Kittle, H. Rushmeier, J. Dorsey, R. O. Prum, and D. J. Brady, "3D imaging spectroscopy for measuring hyperspectral patterns on solid objects," *ACM Trans. Graph. (Proc. SIGGRAPH)*, vol. 31, no. 4, pp. 38:1–11, 2012.

[10] S. K. Nayar, G. Krishnan, M. D. Grossberg, and R. Raskar, "Fast separation of direct and global components of a scene using high frequency illumination," *ACM Trans. Graph. (TOG)*, vol. 25, no. 3, pp. 935–944, 2006.

[11] M. H. Kim and J. Kautz, "Characterization for high dynamic range imaging," *Computer Graphics Forum (Proc. EUROGRAPHICS 2008)*, vol. 27, no. 2, pp. 691–697, 2008.

[12] W. Jakob, "Mitsuba renderer," 2010, http://www.mitsuba-renderer.org.

Giljoo Nam received his master degree in computer science from KAIST and now works as a researcher in the KAIST Visual Computing Laboratory (VCLAB). Prior to KAIST, he received a bachelor degree in Electronic Engineering from Korea University in 2012. His research focuses on hyperspectral photometric stereo imaging. **Address:** Giljoo Nam, Visual Computing Laboratory, KAIST Computer Science Dept., 291 Daehak-ro, Yuseong-gu, Daejeon 305-701, South Korea, gjnam@vclab.kaist.ac.kr

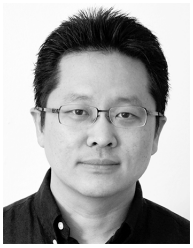

Min H. Kim is an assistant professor of computer science at KAIST, Korea. Prior to KAIST, he worked as a post-doctorial researcher at Yale University. He received his PhD in computer science from University College London (UCL) in 2010. His research interests include color, 3D imaging and visual perception. **Address:** Min H. Kim, Visual Computing Laboratory, KAIST Computer Science Dept., 291 Daehak-ro, Yuseong-gu, Daejeon 305-701, South Korea, minhkim@vclab.kaist.ac.kr